Skeletal Muscle

RESEARCH

Open Access

Neuromuscular electrical stimulation training induces myonuclear accretion and hypertrophy in mice without overt signs of muscle damage and regeneration

Aurélie Fessard[1†], Aliki Zavoriti[1†], Natacha Boyer[1], Jules Guillemaud[1], Masoud Rahmati[1,2], Peggy Del Carmine[1], Christelle Gobet[1], Bénédicte Chazaud[1] and Julien Gondin[1*]

Abstract

Background Skeletal muscle is a plastic tissue that adapts to increased mechanical loading/contractile activity through fusion of muscle stem cells (MuSCs) with myofibers, a physiological process referred to as myonuclear accretion. However, it is still unclear whether myonuclear accretion is driven by increased mechanical loading per se, or occurs, at least in part, in response to muscle injury/regeneration. Here, we developed a non-damaging protocol to evaluate contractile activity-induced myonuclear accretion/hypertrophy in physiological conditions.

Methods Contractile activity was generated by applying repeated electrical stimuli over the mouse plantar flexor muscles. This method is commonly referred to as NeuroMuscular Electrical Simulation (NMES) in Human. Each NMES training session consisted of 80 isometric contractions delivered at ~15% of maximal tetanic force to avoid muscle damage. C57BL/6J male mice were submitted to either a short (*i.e.*, 6 sessions) or long (*i.e.*, 12 sessions) individualized NMES training program while unstimulated mice were used as controls. Histological investigations were performed to assess the impact of NMES on MuSC number and status, myonuclei content and muscle tissue integrity, typology and size.

Results NMES led to a robust proliferation of MuSCs and myonuclear accretion in the absence of overt signs of muscle damage/regeneration. NMES-induced myonuclear accretion was specific to type IIB myofibers and was an early event preceding muscle hypertrophy inasmuch as a mild increase in myofiber cross-sectional area was only observed in response to the long-term NMES training protocol.

Conclusion We conclude that NMES-induced myonuclear accretion and muscle hypertrophy are driven by a mild increase in mechanical loading in the absence of overt signs of muscle injury.

Keywords Muscle stem cells, Skeletal muscle plasticity, Force production, Contractile activity, Resistance training

[†]Aurélie Fessard and Aliki Zavoriti contributed equally to this work.

*Correspondence:
Julien Gondin
Julien.gondin@univ-lyon1.fr
Full list of author information is available at the end of the article

© The Author(s) 2025. **Open Access** This article is licensed under a Creative Commons Attribution-NonCommercial-NoDerivatives 4.0 International License, which permits any non-commercial use, sharing, distribution and reproduction in any medium or format, as long as you give appropriate credit to the original author(s) and the source, provide a link to the Creative Commons licence, and indicate if you modified the licensed material. You do not have permission under this licence to share adapted material derived from this article or parts of it. The images or other third party material in this article are included in the article's Creative Commons licence, unless indicated otherwise in a credit line to the material. If material is not included in the article's Creative Commons licence and your intended use is not permitted by statutory regulation or exceeds the permitted use, you will need to obtain permission directly from the copyright holder. To view a copy of this licence, visit http://creativecommons.org/licenses/by-nc-nd/4.0/.

Background

Skeletal muscle is a remarkably plastic tissue that both regenerates *ad integrum* after an acute injury and adapts to changes in mechanical loading/contractile activity (*e.g.*, disuse, overloading). This plasticity widely relies on muscle stem cells (aka satellite cells, MuSCs) which are located beneath the basal laminal, *i.e.*, at the periphery of the myofibers. While MuSCs are indispensable for muscle regeneration (1–3), during which they exit quiescence, expand, differentiate and fuse to form new functional myofibers, emerging evidence illustrates their roles in skeletal muscle hypertrophy (4).

Over the last few years, it was demonstrated that mechanical overload leads to MuSC fusion with existing myofibers, a physiological process referred to as myonuclear accretion. Thanks to the development of genetic mouse models either ablated for MuSCs (5,6) or deleted for transcription factors involved in MuSC regulation (7,8) or in myofiber homeostasis (9), the requirement of MuSC-mediated myonuclear accretion for hypertrophy was demonstrated in young animals (5–7) and in response to long-term muscle overload (10). However, the interpretation of these pioneering findings is often limited by the use of non-physiological models of muscle overload consisting in either surgical ablation of synergist muscles or tenotomy (6,8). Indeed, the relevance of these models has been questioned regarding the highly variable magnitude of hypertrophy (*i.e.*, + 30 to 200% of muscle mass in 1–3 weeks post-surgery (6,8)), that largely exceeds what can be achieved in humans after resistance training (*i.e.*, + 5–10% of muscle mass after 20–24 weeks of training) (11). Moreover, these models may also lead to muscle injury, illustrated by the presence of myofibers with central nuclei (6). It is therefore unclear whether MuSC fusion is only driven by increased mechanical loading, or due, at least in part, to the confounding effects of overload-induced muscle regeneration (5,8,12).

To overcome these limitations, weighted voluntary wheel running (13,14) or high-intensity interval treadmill (15) protocols were recently introduced to decipher the contribution of MuSCs to exercise-induced myonuclear accretion and/or hypertrophy. Myonuclear accretion occurs early during training (15,16) while MuSC depletion blunts myofiber hypertrophy (16). Although these physiological models of exercise greatly contributed to improve our understanding on the role of MuSCs in skeletal muscle hypertrophy, running activity relies on repeated eccentric muscle contractions where the muscle may be stretched beyond its optimal length (17), potentially leading to muscle damage. In addition, exercise design usually involves the same absolute increment of wheel load (13) or running speed (15) for all mice so that the training load is not adjusted according to the individual performance capacity. The lack of running exercise individualization might further aggravate the extent of muscle damage (15,18). As a consequence, myonuclear accretion-induced muscle hypertrophy might not only be driven by increased mechanical loading, but may occur, at least in part, in response to running exercise-induced muscle injury in these models.

Here, we developed a non-damaging protocol to evaluate contractile activity-induced myonuclear accretion/hypertrophy in physiological conditions. In this context, contractile activity was generated by applying repeated electrical stimuli over the mouse plantar flexor muscles and was carefully monitored in response to each stimulation train and for each trained mouse. This method is commonly referred as to NeuroMuscular Electrical Simulation (NMES) in Human (19,20) and was performed under isometric conditions to avoid muscle damage (21). NMES triggers a robust MuSC proliferation and myonuclear accretion without overt signs of muscle damage/regeneration. We further demonstrated that NMES-induced myonuclear accretion is an early event preceding muscle hypertrophy.

Materials and Methods

Animals

Experiments were conducted on C57BL/6 J males (Janvier Labs, Le Genest-Saint-Isle, France) at 10–12 weeks of age. Mice were housed in an environment-controlled facility (12–12 h light–dark cycle, 25 °C), received water and standard food ad libitum. All of the experiments and procedures were conducted in accordance with French and European legislation on animal experimentation and approved by the ethics committee CEEA-55 and the French ministry of research (APAFIS#12794 and #46817). The experimental protocol included a short-term and a long-term NMES training program described below. According to the ARRIVE guidelines (22), a total of 30 mice was used for the short-term NMES training protocol ($n = 15$ controls and $n = 15$ trained) while a total of 35 mice was used for the long-term NMES program ($n = 15$ controls and $n = 20$ trained).

Experimental device

In order to propose individualized and carefully monitored NMES training protocols, we used a strictly non-invasive ergometer (NIMPHEA_Research, AII Biomedical SAS, Grenoble, France) offering the possibility to electrically stimulate the plantar flexor mouse muscles and to record the resulting force production (Fig. 1A). Mice were initially anesthetized in an induction chamber using 4% isoflurane. The right hindlimb was shaved before an electrode cream was applied over the plantar flexor muscles to optimize electrical stimulation. Each

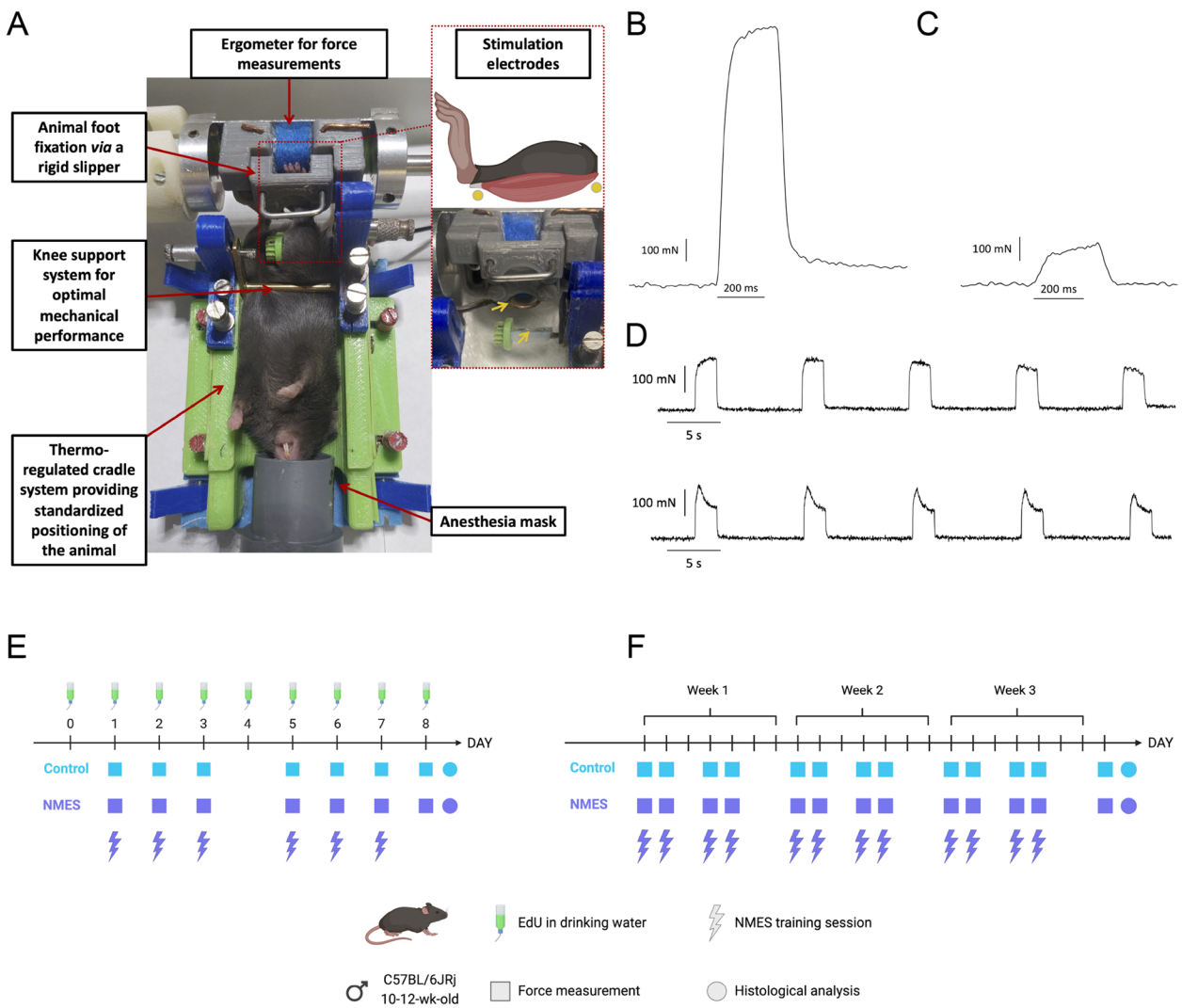

Fig. 1 Experimental setup and design for individualized NMES training protocols. **A** Experimental device allowing for non-invasive longitudinal force measurements and individualized neuromuscular electrical stimulation (NMES) training protocol in response to electrical stimuli applied over the plantar flexor muscle belly. Yellow arrows show the proximal and distal electrodes located below the popliteal fossa and the Achilles tendon, respectively. **B** Typical mechanical trace obtained in response to a 250-ms 100 Hz tetanic stimulation train allowing for maximal isometric force production measurement. **C** Typical mechanical trace obtained in response to a 250-ms 50 Hz subtetanic stimulation train allowing for the determination of the training intensity corresponding to 15% of maximal isometric force. **D** Typical mechanical traces obtained during the first five (top) and last five (bottom) stimulation trains during a typical NMES training session. **E** Schematic representation of the short-term NMES training protocol. C57BL/6 J mice were submitted to either 6 individualized NMES training sessions or a control intervention over a 8-day period. Maximal force production was recorded at the beginning of each NMES or control interventions as well as at day 8. Then, animals were sacrificed and *gastrocnemius* muscle was harvested. A cohort of mice was also treated with 5-ethynyl-2′-deoxyuridine (EdU) in drinking water at the indicated timepoints. **F** Schematic representation of the long-term NMES training protocol. C57BL/6 J mice were submitted to either 12 individualized NMES training sessions or a control intervention over a 3-week period. Maximal force production was recorded at the beginning of each NMES or control interventions as well as at 3 days after the last training session. Then, animals were sacrificed and *gastrocnemius* muscle was harvested

anesthetized mouse was placed supine in a cradle allowing a strict standardization of the animal positioning in ~1 min (Supplemental Video 1). Throughout a typical experiment, anesthesia was maintained by air inhalation through a facemask continuously supplied with 1.5–2.5% isoflurane. The cradle also includes an electrical heating blanket in order to maintain the animal at a physiological temperature during anesthesia. Electrical stimuli were delivered through two electrodes, both being composed of a thin copper wire (width < 1 mm). The proximal electrode was positioned directly on a plastic support that supports the plantar flexor muscles near to the popliteal

fossa. The distal electrode was directly incorporated at the bottom of the foot pedal. Its U-shape allows to stimulate the distal part of the plantar flexor muscles, near the Achilles tendon (Fig. 1A). The right foot was positioned and firmly immobilized through a rigid slipper on a pedal of an ergometer allowing for the measurement of the force produced by the plantar flexor muscles (*i.e.*, mainly the *gastrocnemius* muscle). The right knee was also firmly maintained using a rigid fixation in order to optimize isometric force recordings (Fig. 1A & Supplemental Video 1).

In vivo maximal force measurements and NMES training

Transcutaneous single twitch stimulation was first elicited on the plantar flexor muscles using a constant-current stimulator (Digitimer DS7AH, Hertfordshire, UK; maximal voltage: 400 V; 0.2 ms duration, monophasic rectangular pulses). The individual maximal current intensity was determined by progressively increasing the current intensity until there was no further peak twitch force increase. This intensity was then maintained to measure maximal isometric force production (F_{max}) in response to a 250-ms 100 Hz tetanic stimulation train (Fig. 1B). The maximal current intensity to evoke F_{max} reached a mean value of 133 ± 12 mA.

NMES mice were then submitted to a NMES protocol performed under isometric conditions at a submaximal mechanical intensity corresponding to ~15% of F_{max} in order to i) avoid muscle damage; ii) mimic the application of NMES in severely impaired patients for whom higher force levels are difficult to reach due to discomfort associated with electrical stimuli (23). As a consequence, the current intensity was carefully adjusted at the beginning of each NMES training session in order to reach 15% of F_{max} (*i.e.*, initial intensity $I_{15\%}$; range: 12.5–17.5% of F_{max}) in response to a 250-ms 50 Hz stimulation train (Fig. 1C). Each NMES session consisted of 80 stimulation trains (2-s duration, 8-s recovery) delivered at a frequency of 50 Hz. Every 10 contractions, the current intensity was increased by 50% from $I_{15\%}$ in order to minimize muscle fatigue and maintain a force level of ~15% of F_{max} throughout the NMES protocol (Fig. 1D, Supplemental Fig. 1). For all NMES training sessions and for each mouse, the force produced in response to each stimulation train was quantified, normalized to F_{max} recorded at the beginning of the corresponding session and defined as the training intensity. Control mice were not stimulated but were kept under anesthesia for the same duration as an NMES session. F_{max} was recorded in both NMES and control mice for each training and testing session. Force data was sampled at 1000 Hz with a PowerLab8/35 (ADinstruments, Sydney, Australia) and analyzed with LabChart software (v8.1.17 ADInstruments, Sydney, Australia).

Considering that myonuclear accretion is an early process preceding muscle hypertrophy (15,24), two NMES protocols were designed with different number of training sessions. For the short-term NMES training program (Fig. 1E), NMES mice were stimulated for 2×3 consecutive days separated by one day of rest, for a total of 6 sessions corresponding to a total muscle contractile activity of only 16 min (*i.e.*, 6 sessions × 80 trains × 2 s). A cohort of mice (*i.e.*, $n=5$ controls and $n=4$ trained) was also treated with 5-ethynyl-2'-deoxyuridine (EdU Carbosynth) in drinking water (0.5 mg/ml, 1% glucose) at the indicated timepoints (Fig. 1E) to label proliferating MuSCs. For the long-term NMES training program (Fig. 1F), 12 sessions were performed over a 3 week-period corresponding to a total muscle contractile activity of 32 min (*i.e.*, 12 sessions × 80 trains × 2 s).

Tissue preparation and immunofluorescence analyses

All animals were sacrificed by cervical dislocation after deep isoflurane anesthesia. The right *gastrocnemius* muscle was harvested, weighted and then frozen in isopentane placed in liquid-nitrogen, and kept at −80 °C until use. Cryosections (10 µm) were prepared for immunohistochemical analyses.

Cryosections were permeabilized in Triton-X100 0.5% for 10 min at room temperature, washed 3 times in PBS and then blocked in BSA 4% (except for CD64 staining, BSA 2%) for 1 h at room temperature. Cryosections were then incubated with primary antibodies overnight at 4 °C, washed 3 times (5-min duration) with PBS and further incubated with secondary antibody for 1 h at 37 °C. The following primary antibodies were used: anti-MYH3 (*i.e.*, to label myosin heavy chain embryonic; 1/200, mouse, sc-53091, Santa Cruz Biotech), anti-PCM1 (1/1000, rabbit, HPA023370, Sigma), anti-Laminin (1/200, rabbit, L9393, Merck), anti-Laminin α2 (4H8-2) (1/1000, rat, sc-59854, Santa Cruz Biotech) and anti-CD64 (1/200, rat, 161,002, Biolegend). Secondary antibodies were: Alexa Fluor 488 AffinePure Goat anti-mouse (1/200, ref: 115–545-205), Cy3 AffinePure Donkey anti-rabbit (1/200, ref: 711–165-152), Cy3 AffinePure Donkey anti-mouse (*i.e.*, for determining IgG^{pos} myofibers; 1/200, ref: 715–165-150), Fluorescein (FITC) AffinePure Donkey anti-rabbit (1/200, ref: 711–095–152), and Cy3 AffinePure Donkey Anti-Rat (1/200, ref: 712–165-153) supplied from Jackson ImmunoResearch. Slides were washed with PBS, counterstained with Hoechst and mounted in Fluoromount-G medium.

For myosin heavy chain (MyHC) immunostaining, cryosections were incubated with PBS containing 4% BSA and mouse-on-mouse blocking reagent (1/40,

#MKB-2213, Vector Laboratories) for 1h30 at room temperature. Then, cryosections were incubated with primary antibodies in PBS containing BSA 4% overnight at 4 °C, washed with PBS (50 min), further incubated with secondary antibody for 1 h at 37 °C (BSA 4%) and washed for 50 min in PBS. Slides were mounted in Fluoromount-G medium. The following antibodies were used: anti-MyHC-I (1/50, BA-D5, DSHB), anti-MyHC-IIA (1/50, SC-71, DSHB), anti-MyHC-IIX (1/50, 6H1, DSHB), anti-MyHC-IIB (1/50, BF-F3, DSHB), anti-laminin (1/200, L9393 Sigma), Alexa Fluor 405 IgG2b anti-mouse (1/150, ref: 115–475-207), Alexa Fluor 488 IgG1 anti-mouse (1/150, ref: 115–545-205), Alexa Fluor 546 IgM anti-mouse (1/150, ref: 115–295-020) and Alexa Fluor 647 anti-rabbit (1/200, ref: 711–175-152).

For Pax7 immunostaining, cryosections were first fixed with PFA 4% for 20 min, washed 3 times in PBS, permeabilized in 100% methanol (previously cool down at −20 °C) for 6 min, washed 3 times in PBS, then immerged into citrate buffer 10 mM in 90 °C hot water bath twice 5 min, washed 3 times in PBS and blocked in BSA 4% for 2–3 h. Every step was performed at room temperature, unless indicated otherwise. Cryosections were then incubated with primary antibodies as described above except that anti-Pax7 (1/50, mouse, DSHB) was diluted in blocking buffer containing BSA 4%. Biotin-conjugated donkey anti-mouse IgG1 (1/200, #BA-2000, Vector) was used against Pax7 primary antibody for 1 h at 37 °C then DTAF-conjugated streptavidin (1/1000, ref: 016–010–084, Jackson immunoResearch) was used for 1 h at 37 °C.

EdU detection was performed using Click-iT EdU HCS Assay, according to the manufacturer's instructions (C10350, Invitrogen).

Image capture and analysis

Ten to fifteen images were recorded from each section with an Axio Observer.Z1 (Zeiss) connected to a CoolSNAP HQ2 CCD Camera (photometrics) at 20×magnification for the quantification of the number of $PCM1^{pos}$ nuclei, EdU^{pos} nuclei and $Pax7^{pos}$ cells using ImageJ software. The number of nuclei positive for PCM1 located below the basal lamina (*i.e.*, defined as myonuclei, (25)) was divided by the number of myofibers analyzed on the same picture. The newly fused myonuclei that are derived from cycling MuSCs was assessed by quantifying the number of $PCM1^{pos}EdU^{pos}$cells located below the basal lamina. This number was also divided by the number of myofibers analyzed on the same picture or expressed in relation to the total number of $PCM1^{pos}$ cells. The number of $Pax7^{pos}$ cells and $Pax7^{pos}EdU^{pos}$cells was also divided by the number of myofibers analyzed on the same picture. The number of myonuclei was also determined according to the myofiber type. Ten to fifteen images were recorded from each section with an Axio Observer 7 (Zeiss) connected to an ORCA-Flash4.0 LT3 Digital CMOS camera at 20×magnification. For each myofiber type, nuclei with their geometric center within the inner rim of the laminin ring were defined as myonuclei. These analyses were performed in a blinded manner. For the quantification of the number of $CD64^{pos}$ cells, whole scan images were recorded from each section with an Axio Observer 7 (Zeiss) connected to an ORCA-Flash4.0 LT3 Digital CMOS camera. Then, ten regions of interest of equal surfaces (650 μm^2) were analyzed.

For whole cryosection analysis, slides were automatically scanned at×10 magnification using either an Axio Observer.Z1 (Zeiss) connected to a CoolSNAP HQ2 CCD Camera (photometrics) or an Axio Observer 7 (Zeiss) connected to an ORCA-Flash4.0 LT3 Digital CMOS camera. The image of the whole cryosection was automatically reconstituted in MetaMorph or Zen Pro 3.8 software.

The number of IgG positive myofibers (*i.e.*, based on staining with cy3 anti-mouse), MyHC-embryonic positive myofibers and myofibers with central nuclei were quantified on the whole section and normalized to the total number of myofibers. For the short-term NMES training protocol, myofiber cross-sectional area (CSA) was determined on whole *gastrocnemius* muscle sections labeled by anti-laminin antibody using the OpenCSAM program, as previously described (26). For the long-term NMES training protocol, the myofiber CSA was determined according to the expression of MyHC. Briefly, the automatic segmentation and quantification were performed in Fiji (27) with two lab-made macros and a lab-made Excel template. The first macro included the BIOP-EPFL plugin, which uses the cyto2 deep learning model from the Cellpose algorithm (28), along with the LaRoMe algorithm (https://github.com/BIOP/ijp-LaRoMe) and MorpholibJ plugin (29). The parameters used for Cellpose segmentation were as follows: diameter = 120, cellproba_threshold = 0.0, flow_threshold = 0.4, anisotropy = 3.0, and diam_threshold = 30.0. Additionally, the macro applied an object size filter to remove all labels smaller than 1500 pixels, performed ROI erosion with a radius of 4, and included a code to eliminate artifact ROIs resulting from the label-to-ROI conversion step (LaRoMe). Then, the second macro processed each marker image by splitting and binarizing them using manual thresholding. Manual thresholding was adjusted to ensure that the location of mask signal closely matched the marker staining observed in the original images. The Excel template automatically analyzed the mean intensity value within each myofiber as an indicator of marker positivity. Each mask was binarized with the intensity value ranging from 0 to 255 pixels. Myofibers were classified as

positive for a marker if the mean intensity value within the mask was higher than 85 pixels. To avoid double attributions of cell typology, the final classification was determined by the marker showing the highest mean pixel value. CSA was then determined for each myofiber type.

Statistical Analysis

Statistical analysis was performed using GraphPad Prism Software (version 9.0). Data distribution was initially investigated using Shapiro–Wilk test. Two-factor (group x time) analysis of variance with repeated measures on time was used to compare maximal tetanic force during the short-term NMES training protocol. Two-factor (group x range of CSA) analysis of variance was also used to compare myofiber distribution after long-term NMES training protocol. When a main effect or interaction was observed, a Holm-Šídák post-hoc analysis was performed. Unpaired student t-test or Mann–Whitney was used to assess differences between control and NMES mice for other variables.

Cohen's d effect size and post-hoc power analysis were performed using G-power software (version 3.1.9.6) (30). Overall, the effect size was large ($d \geq 1.08$) for all the variables, although some statistical differences were slightly underpowered (Supplemental Table 1). For each variable, data are presented as mean ± SD (unless indicated) with significance set at $p < 0.05$.

Results

Individualization and monitoring of NMES training program

For both the short- and long-term NMES training programs (Fig. 1E-F), the mean initial current intensity was 1.8 ± 0.6 mA and 1.6 ± 0.5 mA (Supplemental Fig. 1A&E) leading to a mean initial training intensity of 14.1 ± 2.8% F_{max} and 13.5 ± 2.9% F_{max} (Supplemental Fig. 1B&F), respectively. In order to minimize muscle fatigue induced by repeated electrical stimuli, the current intensity was linearly increased every 10 stimulation trains to reach a mean value of 4.9 ± 1.6 mA and 4.5 ± 1.2 mA for the short- and long-term NMES protocols, respectively. Each increment of current intensity resulted in an increase in force production (Supplemental Fig. 1B&F) so that the mean training intensity reached 12.1 ± 2.6% F_{max} and 11.9 ± 2.2% F_{max}. The inter-session variability of both the current and training intensities was relatively low for both the two protocols (CV ranging from 4.1% to 10.5%). Considering that each training session was individualized, we next assessed the intra-group variability for the two NMES training protocols. The mean current intensity typically ranged from 2.8 to 6.9 mA (Supplemental Fig. 1C&G) while the mean training intensity ranged from 9.1 to 16.6% F_{max} (Supplemental Fig. 1D&H). Despite the relatively high intra-group variability of the mean current intensity for the two protocols (*i.e.*, CV of 16.7% and 27.6%), the mean training intensity was less variable within the two groups of trained mice (*i.e.*, CV of 16.2% and 10.1% for the short- and long-term NMES protocols, respectively) (Supplemental Fig. 1D&H).

Overall, our strategy allows for the first time to standardize, individualize and monitor the contractile activity during electrically-evoked isometric contractions at a low force level.

Short-term NMES training triggers the proliferation of MuSCs and promotes MuSC-induced myonuclear accretion

Considering that myonuclear accretion is an early process preceding muscle hypertrophy (15,24), we first designed a short-term NMES training program (Fig. 1E). *Gastrocnemius* muscle was harvested 24 h after the last NMES training session.

Cryosections were first immunostained for Pax7 to label MuSCs in both NMES and control mice (Fig. 2A). The number of $Pax7^{pos}$ cells related to the number of myofibers was higher in NMES mice (+68%, $P < 0.001$) as compared with controls, indicating that NMES increases MuSC content (Fig. 2B). By using EdU tracing, we further assessed the proliferative capacity of MuSCs. We showed that the number of $Pax7^{pos}EdU^{pos}$ cells was higher (+102%; $P < 0.05$) after NMES as compared with controls (Fig. 2C). We next investigated whether NMES could trigger MuSC fusion by counting the number of $PCM1^{pos}$ cells below the basal lamina, defined as myonuclei (25) to avoid the contribution of other cell types (*e.g.*, inflammatory and/or interstitial cells) (31) (Fig. 2D).

(See figure on next page.)

Fig. 2 Effects of short-term NMES training on MuSCs and myonuclear content. **A** Immunostaining for laminin (red), Pax7 (green), EdU (white) and Hoechst (blue) on *gastrocnemius* muscle section from mice submitted either to the control procedure or to NMES. Arrowheads show $Pax7^{pos}EdU^{pos}$ cells. **B** Number of $Pax7^{pos}$ cells *per* myofiber in control ($n = 13$) and NMES ($n = 13$) mice. **C** Number of $Pax7^{pos}EdU^{pos}$ cells *per* myofiber in control ($n = 5$) and NMES ($n = 4$) mice. **D** Immunostaining for laminin (red), PCM1 (green), EdU (white) and Hoechst (blue) on *gastrocnemius* muscle section from mice submitted either to the control procedure or to NMES. Arrowheads show $PCM1^{pos}EdU^{pos}$ cells. **E** Number of myonuclei (*i.e.*, $PCM1^{pos}$ cells below the basal lamina) *per* myofiber in control ($n = 13$) and NMES ($n = 12$) mice. **F** Number of newly fused myonuclei (*i.e.*, $PCM1^{pos}EdU^{pos}$ cells located below the basal lamina) *per* myofiber. **G** Proportion of newly fused myonuclei (% of total $PCM1^{pos}$ cells) in control ($n = 5$) and NMES ($n = 4$) mice. Scale bar = 25 µm. Significantly different from control: $^{*}P < 0.05$; $^{***}P < 0.001$. Values are reported as mean ± SD

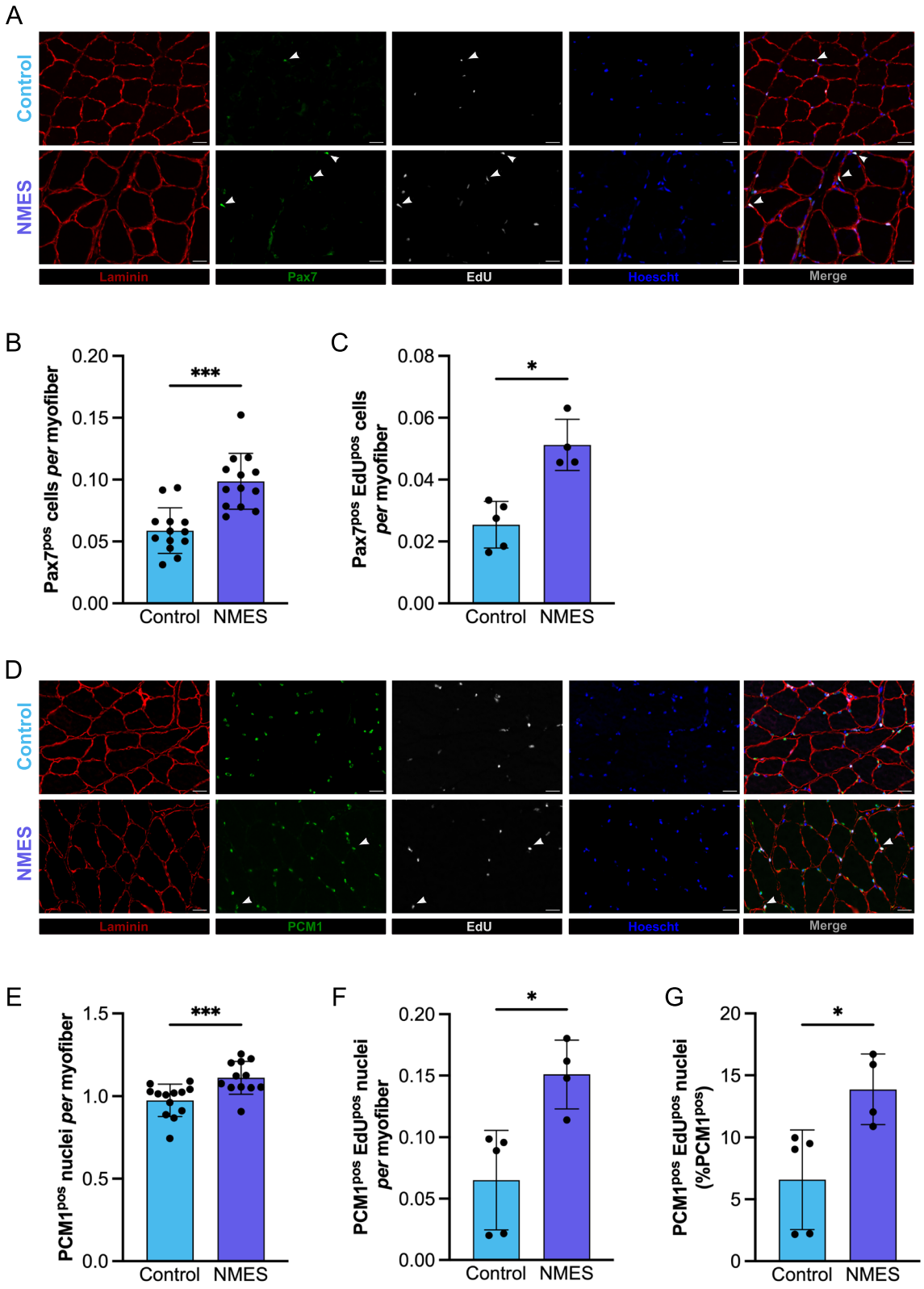

Fig. 2 (See legend on previous page.)

The number of myonuclei *per* myofiber was higher in NMES mice (+14%, $P<0.001$) as compared with controls (Fig. 2E). Finally, we tracked the newly fused myonuclei that are derived from cycling MuSCs by assessing the number of $PCM1^{pos}EdU^{pos}$cells located below the basal lamina. Strikingly, NMES increased ($P<0.05$) the number of $PCM1^{pos}EdU^{pos}$cells *per* myofiber (+132%, Fig. 2F) or related to the total number of $PCM1^{pos}$ cells (+111%, Fig. 2G). In addition, visual inspection of whole *gastrocnemius* sections stained for PCM1 and EdU revealed that EdU positive nuclei were not specifically localized in superficial myofibers but rather dispersed within the *gastrocnemius* muscle (see Supplemental Fig. 2) in NMES trained. Overall, these results demonstrate that a short-term NMES training protocol performed at a mild force level (*i.e.*, ~15% of F_{max}) triggers the proliferation of MuSCs and myonuclear accretion.

Short-term NMES training does not induce overt signs of muscle damage/regeneration

Considering that myonuclear accretion may be driven by muscle damage and/or regeneration (18), we immunostained IgG trapping on *gastrocnemius* cryosections of both NMES and control mice as an index of increased membrane permeability. The proportion of myofibers positive for IgG was negligible in both NMES and control mice (*i.e.*, < 0.2%) (Fig. 3A; Supplemental Fig. 3A-B), showing that NMES did not induce membrane leakage. We also investigated whether signs of muscle regeneration can be observed in *gastrocnemius* muscle of both NMES and control mice. Cryosections were immunostained for MyHC-embryonic (MyHC-emb) that labels newly formed myofibers. The percentage of myofibers positive for MyHC-emb was very low (*i.e.*, < 0.5%) in both control and NMES mice (Fig. 3B; Supplemental Fig. 3C-D). Finally, we counted the number of myofibers with central nuclei, as central positioning of nuclei in myofibers is commonly used as a marker of regeneration (32). In agreement with the MyHC-emb staining, the percentage of myofibers with central nuclei was very low (*i.e.*, < 2%) in all mice (Fig. 3C). On the basis of those three different markers of muscle damage/regeneration, our results illustrate the non-damaging effects of a short-term NMES protocol on *gastrocnemius* muscle.

Upon mechanical overload, MuSC regulation is influenced by different cell types among them macrophages (9,33). We next quantified the number of $CD64^{pos}$ cells, considered as macrophages, in cryosections of both control and NMES trained mice. The number of macrophages was significantly higher ($P<0.05$) in NMES mice (+50%) as compared with controls (Fig. 3D). This indicates that the inflammatory response may be modulated by the contractile activity *per se* and in the absence of overt signs of muscle damage.

Short-term NMES training does not induce muscle hypertrophy or force improvement

Considering that myonuclear accretion has been reported as an early event occurring before (or in absence of) muscle hypertrophy (14,15,24), *gastrocnemius* muscle weight and myofiber CSA were quantified in both control and NMES mice as indices of muscle hypertrophy. These two parameters were not significantly different between control and NMES mice (Fig. 3E-F), indicating that short-term NMES-induced myonuclear accretion was not associated with an increase in muscle mass and myofiber size.

Finally, we investigated whether the changes in both MuSCs and myonuclear content might have a functional effect in terms of muscle force production. Maximal tetanic force (*i.e.*, F_{max}) was recorded longitudinally in both control and NMES mice throughout the duration of the experiment (*i.e.*, Fig. 1E). Our functional analysis reveals that short-term NMES did not increase muscle force (Fig. 3G).

Long-term NMES training promotes myonuclear accretion and muscle hypertrophy in the absence of overt signs of muscle damage/regeneration

On the basis of the myonuclear accretion induced by a short-term NMES training program, we next assessed whether a longer NMES training program could result in muscle hypertrophy in mice (Fig. 1F).

In agreement with the results obtained after short-term NMES training, the number of $Pax7^{pos}$ cells *per* myofiber increased by 55% ($P<0.01$) in NMES mice as compared with controls (Fig. 4A). In the same way, the number of myonuclei *per* myofiber significantly increased by 18% ($P<0.001$) in NMES mice as compared with controls (Fig. 4B). Interestingly, the magnitude of changes for both the number of $Pax7^{pos}$ cells and myonuclei was roughly similar to that observed after short-NMES training, indicating that NMES-induced myonuclear accretion and increase in MuSC content were independent of the training duration. We next assessed whether myonuclear accretion was specific to a myofiber-type. Cryosections were immunostained for laminin, Hoechst, MyHC-I, MyHC-IIA, MyHC-IIX and MyHC-IIB. For each myofiber type, nuclei with their geometric center within the inner rim of the laminin ring were defined as myonuclei. Interestingly, NMES resulted in a significant increase ($P<0.05$) in the number of myonuclei in myofibers expressing MyHC-IIB (+13%; Fig. 4F) while this parameter remains unchanged for the three other myofiber types

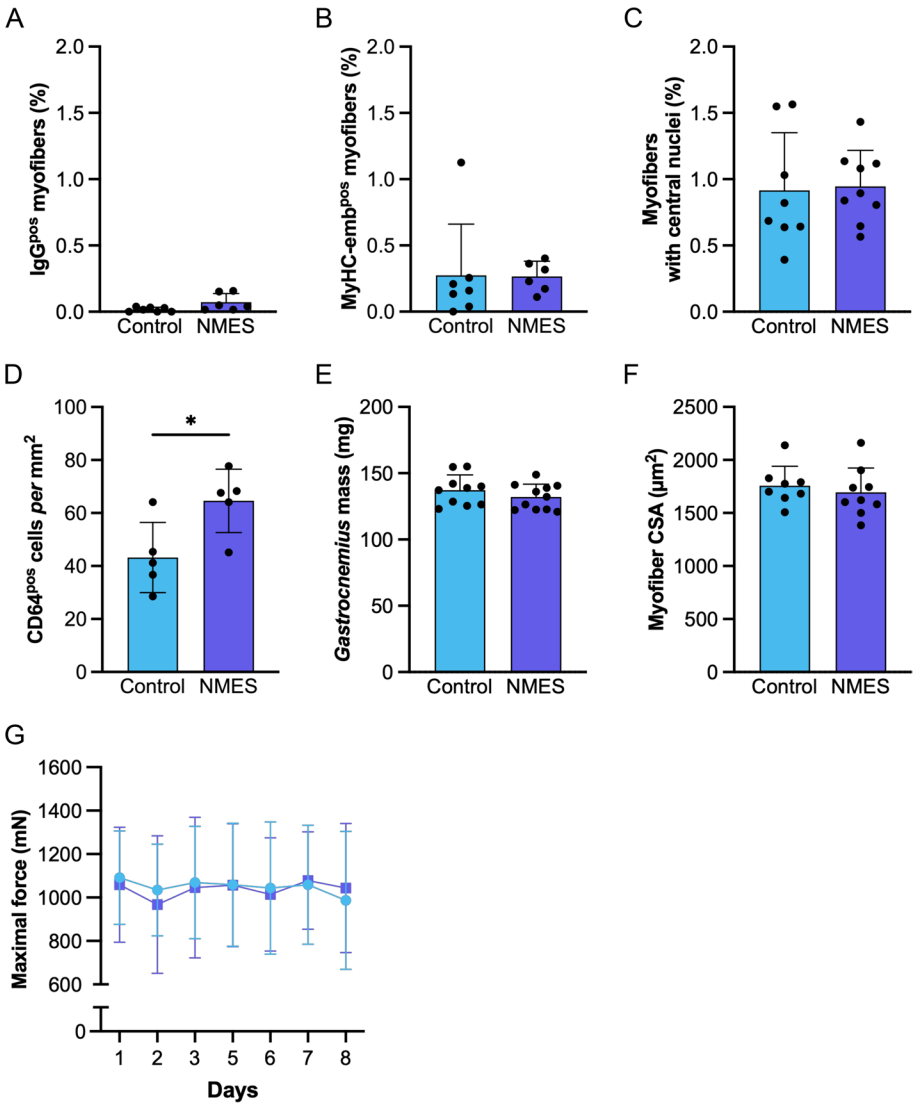

Fig. 3 Effects of short-term NMES training on muscle integrity, macrophage content, muscle mass, size and function. **A** Proportion of myofibers positive for IgG in mice submitted either to the control procedure ($n=7$) or to NMES ($n=6$). **B** Proportion of myofibers positive for myosin heavy chain embryonic in control ($n=7$) and NMES ($n=6$) mice. **C** Proportion of myofibers with central nuclei in control ($n=8$) and NMES ($n=9$) mice. **D** Number of CD64^{pos} cells (*i.e.*, macrophages) *per* mm^2 in control ($n=5$) and NMES ($n=5$) mice. **E** *Gastrocnemius* muscle weight of control ($n=10$) and NMES ($n=11$) mice. **F** *Gastrocnemius* myofiber cross-sectional area of control ($n=8$) and NMES ($n=9$) mice. **G** Maximal isometric force production longitudinally recorded throughout the study design in control ($n=15$; blue circles) and NMES ($n=15$; purple squares) mice. Values are reported as mean ± SD

(See figure on next page.)

Fig. 4 Effects of long-term NMES training on skeletal muscle homeostasis. **A** Number of Pax7^{pos} cells *per* myofiber in control ($n=7$) and NMES ($n=6$) mice. **B** Number of myonuclei (*i.e.*, PCM1^{pos} cells below the basal lamina) *per* myofiber in control ($n=7$) and NMES ($n=6$) mice. **C-F** Number of myonuclei *per* myofiber type I; IIA; IIX and IIB in control ($n=8$) and NMES ($n=8$) mice. **G** *Gastrocnemius* myofiber cross-sectional area distribution in control ($n=15$) and NMES ($n=18$) mice. **H** Whole *gastrocnemius* muscle section immunostained for laminin (grey), MyHC-I (blue), MyHC-IIA (green), MyHC-IIX (black), MyHC-IIB (red). Scale bar = 500 µm. **I-L** Myofiber cross-sectional area of myofiber type I; IIA; IIX and IIB in control ($n=7$) and NMES ($n=11$) mice. **M** Maximal isometric force production in control ($n=15$) and NMES trained ($n=20$) mice. **N** Proportion of myofibers positive for IgG in mice submitted either to the control procedure ($n=7$) or to NMES ($n=6$). **O** Proportion of myofibers positive for embryonic myosin heavy chain in control ($n=7$) and NMES ($n=7$) mice. **P** Proportion of myofibers with central nuclei in control ($n=6$) and NMES ($n=7$) mice. Significantly different from control: $^{*}P<0.05$; $^{**}P<0.01$; $^{***}P<0.001$; $^{\#}P=0.076$; $^{£}P=0.066$. Values are reported as mean ± SD expect for myofiber cross-sectional area distribution where values are reported as mean ± SEM for the sake of clarity

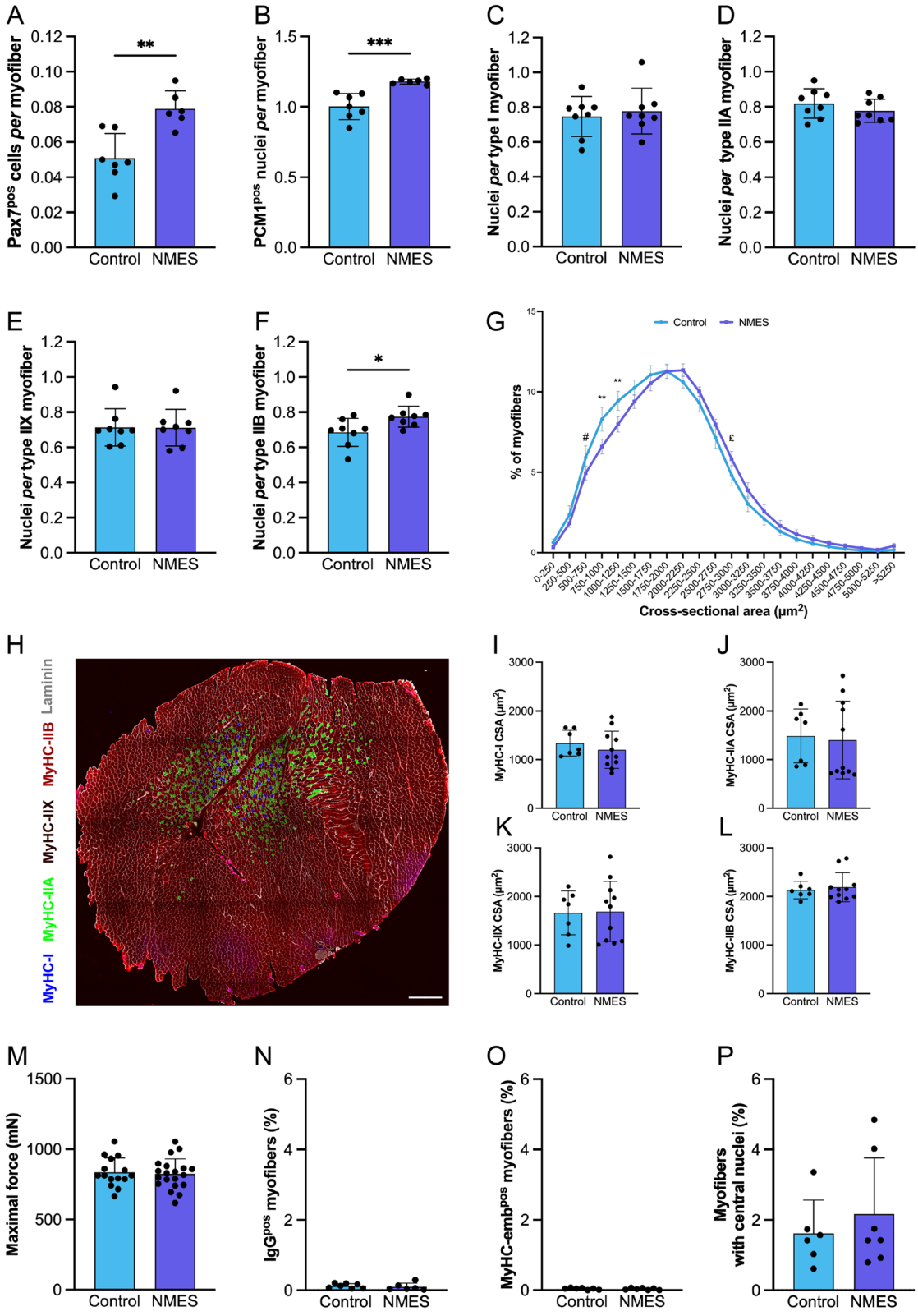

Fig. 4 (See legend on previous page.)

(Fig. 4C-E), thereby illustrating a myofiber-type specificity of myonuclear accretion.

Then, we investigated whether myonuclear accretion induced by the long-term NMES training protocol was associated with muscle hypertrophy. We found that NMES induced a significant shift towards a higher proportion of myofibers with large CSA (Fig. 4G), illustrating a mild muscle hypertrophy. Myofiber CSA was also analyzed according to the expression of MyHC (Fig. 4H). However, the changes were not significant for both type I or type II myofibers (Fig. 4I-L). In addition, no significant changes were observed in both force production (Fig. 4M) and *gastrocnemius* muscle mass (148 ± 16 mg vs. 153 ± 15 mg) between controls and NMES mice.

In agreement with the results obtained in response to the short-term NMES training protocol, the proportion of myofibers positive for IgG or MyHC-emb was negligible (*i.e.*, < 0.3%) in both control and NMES mice (Fig. 4N-O). Finally, the percentage of myofibers with central nuclei was very low (*i.e.*, < 2%; Fig. 4P) and was not significantly different between control and NMES mice. This further confirms the absence of overt signs of muscle injury/regeneration even after a longer NMES training program.

Discussion

In the present study, we took advantage of our original device allowing for non-invasive force measurements in response to electrical stimuli applied over the plantar flexor muscle belly to design individualized and carefully monitored isometric NMES training protocols in mice. We showed that NMES triggers a robust MuSC proliferation and myonuclear accretion without overt signs of muscle damage/regeneration. We further demonstrated that NMES-induced myonuclear accretion is specific to type IIB myofibers and is an early event preceding muscle hypertrophy.

Although the contribution of MuSCs to exercise-induced myonuclear accretion has been well described (5–9), it is still unclear whether this biological effect is driven by increased mechanical loading per se, or occurs, at least in part, in response to muscle injury/regeneration. We demonstrated that an individualized and monitored NMES training protocol performed under isometric conditions at a low force level (*i.e.*, ~15% of F_{max}) did not induce overt signs of muscle damage/regeneration whatever the training duration. Indeed, the proportion of myofibers positive either for IgG labeling or MyHC-emb as well as the percentage of myofibers with central nuclei were very low (*i.e.*, ~ < 2%) after NMES and were never different between control and NMES mice. On the contrary, around 30% of myofibers displayed centrally located nuclei in response to synergist ablation-induced muscle hypertrophy (6). Furthermore, the proportion of myofibers with central nuclei was significantly higher in trained mice as compared with control animals in response to wheel running exercise (14,18) and reached a mean value of ~5–8% (range: ~2–10% in the *soleus* muscle (18)) with (18) or without (14) the co-expression of MyHC-emb. In addition, we showed that NMES did not lead to an acute force reduction (*i.e.*, after a single NMES training session, see Fig. 3G), this parameter being considered as the best indirect marker of muscle damage (34). Overall, while running exercise contains a component of damaging eccentric contractions, an individualized isometric NMES training protocol performed at low force levels (*i.e.*, ~15% of F_{max}) can be considered as a non-damaging modality of increased mechanical loading.

By combining immunostaining analyses with EdU-based tracing, we showed that non-damaging NMES training program increased both MuSC content and the number of proliferating MuSCs. This led to myonuclear accretion as illustrated by the ~14–18% increase in number of myonuclei *per* myofiber together with the large increase (*i.e.*, ~ + 130%) in the number of $PCM1^{pos}EdU^{pos}$cells in NMES mice. Interestingly, the relative increase in myonuclear number was larger and reached ~27–55% after voluntary wheel running (13,14), high-intensity interval treadmill (15) or electrically-evoked eccentric contractions (35). These differences indicate that NMES-induced myonuclear accretion is primarily mediated by the increase in myofiber contractile activity while both muscle overload and damage-related fusion of MuSCs are likely involved in the increased number of myonuclei in response to exercise involving eccentric contractions. Our results also indicate that MuSCs can sense changes in muscle activity and that necrosis, muscle damage and regeneration are not required for MuSC proliferation (8,36). Our findings are in agreement with recent studies showing differences in MuSC dynamics during muscle regeneration and overload (8,37). Indeed, and contrarily to what is usually observed during muscle regeneration, muscle overload leads to MuSC proliferation in the absence of detectable MyoD protein expression (37). It is however noteworthy that these results were obtained in a mouse model of tenotomy which induces a strong mechanical stimulus as illustrated by the large increase in muscle mass (8). In the present study, NMES training was performed at a mild mechanical intensity corresponding to a mean force level of ~15% F_{max}, illustrating the high sensitivity of MuSCs to detect subtle changes in myofiber contractile activity.

The regulation of MuSCs is also influenced by different cell types, among which macrophages (38). Here, we reported that the number of macrophages was 0.5-fold higher in NMES mice as compared with controls.

Interestingly, the macrophage number or concentration was ~ 20-to-26 fold higher in drastic models of muscle hypertrophy (*i.e.*, synergist-ablation, tenotomy) (9,33,39,40) which may also trigger muscle damage/regeneration. Our results clearly indicate that the inflammatory response may be modulated by the contractile activity per se and in the absence of overt signs of muscle damage. However, it remains to determine whether and to what extent the increased number of macrophages contributes to the regulation of MuSCs in response to NMES.

In the present study, contractile activity was generated by applying electrical pulse trains over the mouse plantar flexor muscles while other models of mechanical overload (e.g., synergist ablation, tenotomy, wheel running, treadmill) rely on the repetition of voluntary muscle contractions. Considering the previous in vitro studies showing that the application of electrical pulses in cultured myoblasts strongly influences the different steps (e.g., fusion) (41–43) and/or the molecular actors of myogenesis (e.g., mRNA expression of *MYOD1*) (44), we could assume that electrical current per se might have a direct effect of MuSCs. It should however keep in mind that these in vitro studies do not necessarily reflect the behavior of MuSCs in vivo inasmuch as myofiber-attached MuSCs display different electrophysiological properties (e.g., resting membrane potential) as compared with dissociated MuSCs and myoblasts (45,46). In our opinion, it seems highly difficult to discriminate the role of electrical current from the contribution of muscle contraction on MuSC fusion in vivo. Indeed, considering that NMES triggers muscle contractions via the activation of intramuscular nerve branches (47,48), we could use a neuromuscular transmission blocker (*e.g.*, curare) to prevent muscle contraction and therefore assess the effects of electrical current per se on MuSC fusion. However, such experiments would require repeated anesthesia and mechanical ventilation to allow breathing of mice during NMES application which is technically not feasible. The use of current intensities below the motor threshold could be viewed as another strategy to prevent contractile activity. However, and despite their limitations, in vitro studies showed that the stimulation parameters (e.g., current intensity, stimulation frequency) impact the regulation of myoblasts (49). On that basis, even if low current intensity (< motor threshold) promotes MuSC fusion in vivo independently of muscle contractility, it would not be possible to extrapolate on the behavior of MuSCs in response to current intensity above the motor threshold. Further human investigations would allow to address this question by comparing myonuclear accretion in response to voluntary *vs.* electrically-evoked muscle contractions performed at a similar and low mechanical intensity to mimic the present experiments.

We further demonstrated that NMES-induced myonuclear accretion is an early event occurring before muscle hypertrophy. Indeed, while mice submitted to the short-term NMES training protocol showed an increase in the number of myonuclei without any changes in myofiber CSA, the longer NMES training protocol led to both myonuclear accretion and a significant increase in the proportion of myofibers with large CSA. This is in agreement with previous studies showing that myonuclear accretion precedes muscle hypertrophy in response to mechanical overload (24) or treadmill exercise (7). So far, conflicting findings have been reported on the impact of NMES on muscle hypertrophy in mice as illustrated by the reduction of muscle mass and a decrease in myofiber CSA (50), a mild increase in muscle mass (51) or a significant increase in myofiber CSA (52). These discrepancies could be related to the use of different training intensities (e.g., > 50% of F_{max}) (52) and/or the application of NMES-induced lengthening contractions that could both trigger muscle damage (50). We conclude that our NMES training protocol triggers a mild muscle hypertrophy inasmuch as the magnitude of changes in CSA distribution is much lower than what has been previously reported in drastic models of muscle hypertrophy (*i.e.*, synergist-ablation, tenotomy) (5,6,9).

In agreement with the mild increase in myofiber CSA, maximal force production remained unchanged after NMES. It has been previously reported that changes in myofiber size/mass do not necessarily translate into increase in force production (53–55), especially when resistance training is performed at submaximal intensity (e.g., 15% of maximal force) (53). We also found that EdU positive nuclei were not specifically localized in superficial myofibers but rather dispersed within the *gastrocnemius* muscle (see Supplemental Fig. 2) in NMES trained. We assumed that EdU positive nuclei are localized near to the activated muscle areas. In addition, NMES resulted in myonuclear accretion which was specific to type IIB myofibers. Therefore, NMES mainly activates a limited number of type IIB myofibers independently of their spatial location within the activated *gastrocnemius* muscle. This partial and rather dispersed activation of *gastrocnemius* myofibers during NMES may also explain why the force production remains unchanged after training.

Our NMES training protocol could be of interest to further improve our understanding on the role of muscle memory in the context of muscle adaptations, *i.e.*, to assess whether myonuclei gained during (or in the absence of) hypertrophy are lost during detraining (56–59). Moreover, recent lineage tracing approaches not only revealed distinct transcriptional signatures of newly

fused myonuclei as compared with pre-existing myonuclei but also interactions between these two myonuclear populations to regulate myofiber size in a drastic model of hypertrophy (60). In this study, newly fused myonuclei were mainly located in the center of myofibers, illustrating an ongoing regeneration process. In that context, the use of NMES-induced non damaging muscle contractions could provide key information on how and to what extent the transcriptional responses differ between newly acquired and pre-existing myonuclei located in the periphery of the myofibers. Finally, the training intensity (*i.e.*, 15% of F_{max}) was selected to mimic the application of NMES in severely impaired patients (23) for whom higher force levels are difficult to reach due to discomfort associated with electrical stimuli (61). On that basis, NMES could be relevant to promote myonuclear accretion and hypertrophy in pathological conditions associated with MuSC defects and muscle atrophy (e.g., cancer cachexia, sepsis…) (62,63).

As a proof-of-concept study illustrating the non-damaging effects of NMES on myonuclear accretion and hypertrophy, experiments were conducted on C57BL/6 J males only. Further studies are needed to evaluate whether and to what extent NMES-induced myonuclear accretion and hypertrophy differ between males and females. This is of interest since sex may impact the regulation of MuSCs (64,65).

Conclusion

Our study brings a novel brick in the long-standing debate on MuSC dynamics during muscle regeneration and hypertrophy. We provide strong evidence regarding the sensitivity of MuSCs to detect subtle changes in myofiber contractile activity inasmuch as our NMES training program was performed at a mild mechanical intensity corresponding to a mean force level of ~15% F_{max}. This indicates that neither a strong mechanical stimulus (such as that induced by synergist ablation or tenotomy) nor necrosis/massive damage are required for MuSC expansion and fusion with existing and undamaged myofibers. Further human investigations could also allow to decipher the potential activation of MuSCs by the electrical current itself.

Abbreviations

BSA	Bovine Serum Albumin
CSA	Cross-sectional area
Cy3	Cyanine 3
EdU	5-Ethynyl-2′-deoxyuridine
MyHC-emb	Myosin heavy chain embryonic
F_{max}	Maximal isometric force
IgG	Immunoglobulin G
MuSCs	Muscle stem cells
MYH3	Myosin heavy chain 3
NMES	Neuromuscular electrical stimulation
PBS	Phosphate Buffer Saline
PCM1	Pericentriolar Material 1

Supplementary Information

The online version contains supplementary material available at https://doi.org/10.1186/s13395-024-00372-0.

Supplemental Figure 1. Monitoring of force production during short- and long-term NMES training. A-B) Mean current intensity (in mA) and mean training intensity (expressed in percentage of maximal isometric force) obtained during each of the 6 NMES sessions (*i.e.*, from S1 to S6; mean of 15 mice). Values are reported as mean ± SEM. C-D) Individual current intensity (in mA) and individual training intensity (expressed in percentage of maximal isometric force) throughout the 80 stimulation trains (n=15 mice) of the short-term NMES training protocol (mean of the 6 sessions). Each symbol represents an individual mouse. For the sake of clarity, only mean values are reported. E-F) Mean current intensity (in mA) and mean training intensity (expressed in percentage of maximal isometric force) obtained during each of the 12 NMES sessions (*i.e.*, from S1 to S12; mean of 20 mice). Note that session #8 of one mouse was not recorded due to technical issue. Values are reported as mean ± SEM. G-H) Individual current intensity (in mA) and individual training intensity (expressed in percentage of maximal isometric force) throughout the 80 stimulation trains (n=20 mice) of the long-term NMES training protocol (mean of the 12 sessions). Each symbol represents an individual mouse. For the sake of clarity, only mean values are reported.

Supplemental Figure 2. Effects of NMES on the spatial distribution of EdU positive nuclei. A-B) Immunostaining for PCM1 (purple) and EdU (green) on the whole *gastrocnemius* muscle section from control and NMES trained mice. Scale bar = 100 µm.

Supplemental Figure 3. Effects of NMES on muscle integrity. A-B) Immunostaining for IgG (red) and laminin (green) on *gastrocnemius* muscle section from control and NMES trained mice. Scale bar = 250 µm. C-D) Immunostaining for laminin (red) and myosin heavy chain embryonic (green) on *gastrocnemius* muscle section from control and NMES trained mice. Scale bar = 250 µm.

Acknowledgements

We thank Dr Rémi Mounier and Dr Anita Kneppers for their useful comments on a previous version of the manuscript.

Authors' contributions

Concept/idea/research design: J. Gondin. Writing: J. Gondin. Data collection: A. Zavoriti, A. Fessard, M. Rahmati, N. Boyer, J. Guillemaud, P. Del Carmine, J. Gondin. Data analysis: A. Zavoriti, A. Fessard, N. Boyer, J. Guillemaud, C. Gobet, P. Del Carmine, J. Gondin. Project management: J. Gondin. Consultation (including review of manuscript before submitting): A. Zavoriti, A. Fessard, N. Boyer, J. Guillemaud, C. Gobet, P. Del Carmine, B. Chazaud, J. Gondin. All the authors read and approved the final version of manuscript. Masoud Rahmati acted as a visiting scientist at INMG (from September 2019 to July 2020) where he was trained to NMES training protocol and muscle analysis.

Funding

This study was supported by Partenariats Hubert Curien (PHC)—Programme GUNDISHAPUR 2020, Oncostarter – Cancéropôle CLARA, and AFM-TELETHON (Alliance MyoNeurALP).

Data availability

The datasets used and/or analyzed during the current study are available from the corresponding author on reasonable request.

Declarations

Ethics approval and consent to participate
All of the experiments and procedures were conducted in accordance with French and European legislations on animal experimentation and approved by the local ethic committee CEEA-55 and the French ministry of research (APAFIS#12794 and #46817).

Consent for publication
Not applicable.

Competing interests
The authors declare no competing interests.

Author details
[1]Institut NeuroMyoGène (INMG), Unité Physiopathologie et Génétique du Neurone et du Muscle, Université Claude Bernard Lyon 1, CNRS UMR 5261, Inserm U1315, 8 Avenue Rockefeller, Lyon, France. [2]Department of Exercise Physiology, Faculty of Literature and Human Sciences, Lorestan University, Khoramabad, Iran.

Received: 19 December 2023 Accepted: 23 December 2024
Published online: 05 February 2025

References

1. Lepper C, Partridge TA, Fan CM. An absolute requirement for Pax7-positive satellite cells in acute injury-induced skeletal muscle regeneration. Development. 2011Sep;138(17):3639–46.
2. Murphy MM, Lawson JA, Mathew SJ, Hutcheson DA, Kardon G. Satellite cells, connective tissue fibroblasts and their interactions are crucial for muscle regeneration. Development. 2011Sep;138(17):3625–37.
3. Sambasivan R, Yao R, Kissenpfennig A, Van Wittenberghe L, Paldi A, Gayraud-Morel B, et al. Pax7-expressing satellite cells are indispensable for adult skeletal muscle regeneration. Development. 2011Sep;138(17):3647–56.
4. Murach KA, Fry CS, Dupont-Versteegden EE, McCarthy JJ, Peterson CA. Fusion and beyond: Satellite cell contributions to loading-induced skeletal muscle adaptation. FASEB J. 2021Oct;35(10): e21893.
5. Egner IM, Bruusgaard JC, Gundersen K. Satellite cell depletion prevents fiber hypertrophy in skeletal muscle. Development. 2016Aug 15;143(16):2898–906.
6. McCarthy JJ, Mula J, Miyazaki M, Erfani R, Garrison K, Farooqui AB, et al. Effective fiber hypertrophy in satellite cell-depleted skeletal muscle. Development. 2011Sep 1;138(17):3657–66.
7. Goh Q, Millay DP. Requirement of myomakermediated stem cell fusion for skeletal muscle hypertrophy. eLife. 2017;6:e20007.
8. Fukuda S, Kaneshige A, Kaji T, Noguchi YT, Takemoto Y, Zhang L, et al. Sustained expression of HeyL is critical for the proliferation of muscle stem cells in overloaded muscle. Elife. 2019Sep;23(8): e48284.
9. Noviello C, Kobon K, Delivry L, Guilbert T, Britto F, Julienne F, et al. RhoA within myofibers controls satellite cell microenvironment to allow hypertrophic growth. IScience. 2022;25(1):103616.
10. Fry CS, Lee JD, Jackson JR, Kirby TJ, Stasko SA, Liu H, et al. Regulation of the muscle fiber micro environment by activated satellite cells during hypertrophy. FASEB j. 2014Apr;28(4):1654–65.
11. Reggiani C, Schiaffino S. Muscle hypertrophy and muscle strength: dependent or independent variables? A provocative review. Eur J Transl Myol. 2020Sep 30;30(3):9311.
12. Murach KA, White SH, Wen Y, Ho A, Dupont-Versteegden EE, McCarthy JJ, et al. Differential requirement for satellite cells during overload-induced muscle hypertrophy in growing versus mature mice. Skelet Muscle. 2017Jul 10;7(1):14.
13. Dungan CM, Murach KA, Frick KK, Jones SR, Crow SE, Englund DA, et al. Elevated myonuclear density during skeletal muscle hypertrophy in response to training is reversed during detraining. Am J Physiol, Cell Physiol. 2019May 1;316(5):C649–54.
14. Masschelein E, D'Hulst G, Zvick J, Hinte L, Soro-Arnaiz I, Gorski T, et al. Exercise promotes satellite cell contribution to myofibers in a load-dependent manner. Skelet Muscle. 2020Jul 9;10(1):21.
15. Goh Q, Song T, Petrany MJ, Cramer AA, Sun C, Sadayappan S, et al. Myonuclear accretion is a determinant of exercise-induced remodeling in skeletal muscle. Elife. 2019Apr;23(8): e44876.
16. Englund DA, Figueiredo VC, Dungan CM, Murach KA, Peck BD, Petrosino JM, et al. Satellite Cell Depletion Disrupts Transcriptional Coordination and Muscle Adaptation to Exercise. Function (Oxf). 2021;2(1):zqaa033.
17. Katz B. The relation between force and speed in muscular contraction. J Physiol. 1939Jun 14;96(1):45–64.
18. Murach KA, Mobley CB, Zdunek CJ, Frick KK, Jones SR, McCarthy JJ, et al. Muscle memory: myonuclear accretion, maintenance, morphology, and miRNA levels with training and detraining in adult mice. J Cachexia Sarcopenia Muscle. 2020Dec;11(6):1705–22.
19. Gondin J, Guette M, Ballay Y, Martin A. Electromyostimulation training effects on neural drive and muscle architecture. Med Sci Sports Exerc. 2005;37(8):1291–9.
20. Gondin J, Brocca L, Bellinzona E, D'Antona G, Maffiuletti NA, Miotti D, et al. Neuromuscular electrical stimulation training induces atypical adaptations of the human skeletal muscle phenotype: a functional and proteomic analysis. J Appl Physiol. 2011Feb;110(2):433–50.
21. Gondin, Giannesini B, Vilmen C, Le Fur Y, Cozzone PJ, Bendahan D. Effects of a single bout of isometric neuromuscular electrical stimulation on rat gastrocnemius muscle: a combined functional, biochemical and MRI investigation. J Electromyogr Kinesiol. 2011 Jun;21(3):525–32.
22. Percie du Sert N, Hurst V, Ahluwalia A, Alam S, Avey MT, Baker M, et al. The ARRIVE guidelines 20 Updated guidelines for reporting animal research. PLoS Biol. 2020;18(7):e3000410.
23. Maddocks M, Nolan CM, Man WDC, Polkey MI, Hart N, Gao W, et al. Neuromuscular electrical stimulation to improve exercise capacity in patients with severe COPD: a randomised double-blind, placebo-controlled trial. Lancet Respir Med. 2016Jan;4(1):27–36.
24. Bruusgaard JC, Johansen IB, Egner IM, Rana ZA, Gundersen K. Myonuclei acquired by overload exercise precede hypertrophy and are not lost on detraining. Proc Natl Acad Sci U S A. 2010Aug 24;107(34):15111–6.
25. Winje IM, Bengtsen M, Eftestøl E, Juvkam I, Bruusgaard JC, Gundersen K. Specific labelling of myonuclei by an antibody against pericentriolar material 1 on skeletal muscle tissue sections. Acta Physiol (Oxf). 2018Aug;223(4): e13034.
26. Desgeorges T, Liot S, Lyon S, Bouvière J, Kemmel A, Trignol A, et al. Open-CSAM, a new tool for semi-automated analysis of myofiber cross-sectional area in regenerating adult skeletal muscle. Skelet Muscle. 2019;9(1):2.
27. Schindelin J, Arganda-Carreras I, Frise E, Kaynig V, Longair M, Pietzsch T, et al. Fiji: an open-source platform for biological-image analysis. Nat Methods. 2012Jun 28;9(7):676–82.
28. Stringer C, Wang T, Michaelos M, Pachitariu M. Cellpose: a generalist algorithm for cellular segmentation. Nat Methods. 2021Jan;18(1):100–6.
29. Legland D, Arganda-Carreras I, Andrey P. MorphoLibJ: integrated library and plugins for mathematical morphology with ImageJ. Bioinformatics. 2016Nov 15;32(22):3532–4.
30. Faul F, Erdfelder E, Buchner A, Lang AG. Statistical power analyses using G*Power 3.1: tests for correlation and regression analyses. Behav Res Methods. 2009;41(4):1149–60.
31. Viggars MR, Owens DJ, Stewart C, Coirault C, Mackey AL, Jarvis JC. PCM1 labeling reveals myonuclear and nuclear dynamics in skeletal muscle across species. Am J Physiol Cell Physiol. 2023Jan 1;324(1):C85-97.
32. Matsuda R, Spector DH, Strohman RC. Regenerating adult chicken skeletal muscle and satellite cell cultures express embryonic patterns of myosin and tropomyosin isoforms. Dev Biol. 1983Dec;100(2):478–88.
33. DiPasquale DM, Cheng M, Billich W, Huang SA, van Rooijen N, Hornberger TA, et al. Urokinase-type plasminogen activator and macrophages are required for skeletal muscle hypertrophy in mice. Am J Physiol Cell Physiol. 2007Oct;293(4):C1278–85.
34. Warren GL, Lowe DA, Armstrong RB. Measurement tools used in the study of eccentric contraction-induced injury. Sports Med. 1999Jan;27(1):43–59.
35. Viggars MR, Wen Y, Peterson CA, Jarvis JC. Automated cross-sectional analysis of trained, severely atrophied, and recovering rat skeletal muscles using MyoVision 2.0. J Appl Physiol (1985). 2022;132(3):593–610.

36. Darr KC, Schultz E. Exercise-induced satellite cell activation in growing and mature skeletal muscle. J Appl Physiol (1985). 1987;63(5):1816–21.
37. Fukada SI, Higashimoto T, Kaneshige A. Differences in muscle satellite cell dynamics during muscle hypertrophy and regeneration. Skelet Muscle. 2022Jul 6;12(1):17.
38. Bernard C, Zavoriti A, Pucelle Q, Chazaud B, Gondin J. Role of macrophages during skeletal muscle regeneration and hypertrophy-Implications for immunomodulatory strategies. Physiol Rep. 2022Oct;10(19): e15480.
39. Marino JS, Tausch BJ, Dearth CL, Manacci MV, McLoughlin TJ, Rakyta SJ, et al. β 2 -Integrins contribute to skeletal muscle hypertrophy in mice. Am J Physiol Cell Physiol. 2008Oct;295(4):C1026–36.
40. Zhang L, Saito H, Higashimoto T, Kaji T, Nakamura A, Iwamori K, et al. Regulation of muscle hypertrophy through granulin: Relayed communication among mesenchymal progenitors, macrophages, and satellite cells. Cell Rep. 2024Apr 23;43(4): 114052.
41. Entwistle A, Zalin RJ, Bevan S, Warner AE. The control of chick myoblast fusion by ion channels operated by prostaglandins and acetylcholine. J Cell Biol. 1988May;106(5):1693–702.
42. Bernheim L, Liu JH, Hamann M, Haenggeli CA, Fischer-Lougheed J, Bader CR. Contribution of a non-inactivating potassium current to the resting membrane potential of fusion-competent human myoblasts. J Physiol. 1996May 15;493(Pt 1):129–41.
43. Khodabukus A, Madden L, Prabhu NK, Koves TR, Jackman CP, Muoio DM, et al. Electrical stimulation increases hypertrophy and metabolic flux in tissue-engineered human skeletal muscle. Biomaterials. 2019Apr;198:259–69.
44. Scheler M, Irmler M, Lehr S, Hartwig S, Staiger H, Al-Hasani H, et al. Cytokine response of primary human myotubes in an in vitro exercise model. Am J Physiol Cell Physiol. 2013Oct 15;305(8):C877-886.
45. Cossu G, Eusebi F, Grassi F, Wanke E. Acetylcholine receptor channels are present in undifferentiated satellite cells but not in embryonic myoblasts in culture. Dev Biol. 1987Sep;123(1):43–50.
46. Bader CR, Bertrand D, Cooper E, Mauro A. Membrane currents of rat satellite cells attached to intact skeletal muscle fibers. Neuron. 1988May;1(3):237–40.
47. Hultman E, Sjoholm H, Jaderholm-Ek I, Krynicki J. Evaluation of methods for electrical stimulation of human skeletal muscle in situ. Pflugers Arch. 1983;398(2):139–41.
48. Yamaguchi T, Kouzaki K, Sasaki K, Nakazato K. Alterations in neuromuscular junction morphology with ageing and endurance training modulate neuromuscular transmission and myofibre composition. J Physiol. 2025;603(1):107–25.
49. Nikolić N, Görgens SW, Thoresen GH, Aas V, Eckel J, Eckardt K. Electrical pulse stimulation of cultured skeletal muscle cells as a model for in vitro exercise - possibilities and limitations. Acta Physiol (Oxf). 2017Jul;220(3):310–31.
50. Viggars MR, Sutherland H, Cardozo CP, Jarvis JC. Conserved and species-specific transcriptional responses to daily programmed resistance exercise in rat and mouse. FASEB J. 2023Dec;37(12): e23299.
51. Lotri-Koffi A, Pauly M, Lemarié E, Godin-Ribuot D, Tamisier R, Pépin JL, et al. Chronic neuromuscular electrical stimulation improves muscle mass and insulin sensitivity in a mouse model. Sci Rep. 2019May 10;9(1):7252.
52. Eftestøl E, Egner IM, Lunde IG, Ellefsen S, Andersen T, Sjåland C, et al. Increased hypertrophic response with increased mechanical load in skeletal muscles receiving identical activity patterns. Am J Physiol Cell Physiol. 2016Oct 1;311(4):C616–29.
53. Kacin A, Strazar K. Frequent low-load ischemic resistance exercise to failure enhances muscle oxygen delivery and endurance capacity. Scand J Med Sci Sports. 2011Dec;21(6):e231-241.
54. Jakobsgaard JE, Christiansen M, Sieljacks P, Wang J, Groennebaek T, de Paoli F, et al. Impact of blood flow-restricted bodyweight exercise on skeletal muscle adaptations. Clin Physiol Funct Imaging. 2018. p. 965–75
55. Loenneke JP, Buckner SL, Dankel SJ, Abe T. Exercise-Induced Changes in Muscle Size do not Contribute to Exercise-Induced Changes in Muscle Strength. Sports Med. 2019Jul 1;49(7):987–91.
56. Kirby TJ, Dupont-Versteegden EE. Cross Talk proposal: Myonuclei are lost with ageing and atrophy. J Physiol. 2022May;600(9):2077–80.
57. Schwartz LM, Gundersen K. Cross Talk opposing view: Myonuclei do not undergo apoptosis during skeletal muscle atrophy. J Physiol. 2022May;600(9):2081–4.
58. Snijders T, Aussieker T, Holwerda A, Parise G, van Loon LJC, Verdijk LB. The concept of skeletal muscle memory: Evidence from animal and human studies. Acta Physiol (Oxf). 2020Jul;229(3): e13465.
59. Venturelli M, Schena F, Naro F, Reggiani C, Pereira Guimarães M, de Almeida Costa Campos Y, et al. Commentaries on Viewpoint: "Muscle memory" not mediated by myonuclear number? Secondary analysis of human detraining data. J Appl Physiol. 2019;127(6):1817–20.
60. Sun C, Swoboda CO, Morales FM, Calvo C, Petrany MJ, Parameswaran S, et al. Lineage tracing of nuclei in skeletal myofibers uncovers distinct transcripts and interplay between myonuclear populations. Nat Commun. 2024Oct;30(15):9372.
61. Gondin J, Cozzone PJ, Bendahan D. Is high-frequency neuromuscular electrical stimulation a suitable tool for muscle performance improvement in both healthy humans and athletes? Eur J Appl Physiol. 2011Oct;111(10):2473–87.
62. He WA, Berardi E, Cardillo VM, Acharyya S, Aulino P, Thomas-Ahner J, et al. NF-κB-mediated Pax7 dysregulation in the muscle microenvironment promotes cancer cachexia. J Clin Invest. 2013Nov;123(11):4821–35.
63. Rocheteau P, Chatre L, Briand D, Mebarki M, Jouvion G, Bardon J, et al. Sepsis induces long-term metabolic and mitochondrial muscle stem cell dysfunction amenable by mesenchymal stem cell therapy. Nat Commun. 2015;6:10145.
64. Deasy BM, Lu A, Tebbets JC, Feduska JM, Schugar RC, Pollett JB, et al. A role for cell sex in stem cell-mediated skeletal muscle regeneration: female cells have higher muscle regeneration efficiency. J Cell Biol. 2007Apr 9;177(1):73–86.
65. Jomard C, Gondin J. Influence of sexual dimorphism on satellite cell regulation and inflammatory response during skeletal muscle regeneration. Physiol Rep. 2023Oct;11(19): e15798.

Publisher's Note

Springer Nature remains neutral with regard to jurisdictional claims in published maps and institutional affiliations.